Eur Biophys J (2005) 34: 97–112
DOI 10.1007/s00249-004-0434-z

ARTICLE

**Matthias Mentler · Andreas Weiss · Klaus Grantner
Pablo del Pino · Dominga Deluca · Stella Fiori
Christian Renner · Wolfram Meyer Klaucke
Luis Moroder · Uwe Bertsch · Hans A. Kretzschmar
Paul Tavan · Fritz G. Parak**

A new method to determine the structure of the metal environment in metalloproteins: investigation of the prion protein octapeptide repeat Cu^{2+} complex

Received: 29 May 2004 / Revised: 2 July 2004 / Accepted: 5 July 2004 / Published online: 28 September 2004

Abstract Since high-intensity synchrotron radiation is available, ''extended X-ray absorption fine structure'' spectroscopy (EXAFS) is used for detailed structural analysis of metal ion environments in proteins. However, the information acquired is often insufficient to obtain an unambiguous picture. ENDOR spectroscopy allows the determination of hydrogen positions around a metal ion. However, again the structural information is limited. In the present study, a method is proposed which combines computations with spectroscopic data from EXAFS, EPR, electron nuclear double resonance (ENDOR) and electron spin echo envelope modulation (ESEEM). From EXAFS a first picture of the nearest coordination shell is derived which has to be compatible with EPR data. Computations are used to select sterically possible structures, from which in turn structures with correct H and N positions are selected by ENDOR and ESEEM measurements. Finally, EXAFS spectra are re-calculated and compared with the experimental data. This procedure was successfully applied for structure determination of the Cu^{2+} complex of the octapeptide repeat of the human prion protein. The structure of this octarepeat complex is rather similar to a pentapeptide complex which was determined by X-ray structure analysis. However, the tryptophan residue has a different orientation: the axial water is on the other side of the Cu.

Keywords Electron nuclear double resonance · Electron spin echo envelope modulation · Extended X-ray absorption fine structure spectroscopy · Prion protein · Protein structure

M. Mentler · K. Grantner · P. del Pino · F. G. Parak (✉)
Physik-Department E17,
Technische Universität München,
85747 Garching, Germany
E-mail: fritz.parak@ph.tum.de
Tel.: +49-89-28912551
Fax: +49-89-28912548

A. Weiss · P. Tavan
Lehrstuhl für Biomolekulare Optik,
Ludwig-Maximilians-Universität München,
Oettingenstrasse 67, 80538 Munich, Germany

D. Deluca · S. Fiori · C. Renner · L. Moroder
Max-Planck-Institut für Biochemie,
82152 Martinsried, Germany

W. M. Klaucke
EMBL, c/o DESY, Notkestrasse 85,
22603 Hamburg, Germany

U. Bertsch · H. A. Kretzschmar
Institut für Neuropathologie,
Ludwig-Maximilians-Universität München,
80538 Munich, Germany

Introduction

NMR represents the most important experimental method for the structural analysis of peptides and proteins for which single crystals are not available (Wüthrich 2003). NMR structure determination relies on a combination of experimentally determined distance restraints with a molecular mechanics (MM) force field, which adds expertise to the structures and flexibilities of the chemical building blocks of proteins. Simulated annealing strategies then serve to solve the complicated optimization problem of combining all this information into a three-dimensional structure (Brünger et al. 1987). In NMR, special care is required if the protein contains a paramagnetic metal ion (Arnesano et al. 2003a). Therefore, alternative approaches towards structure determination should be established for these cases.

In fact, a series of other spectroscopic methods has been successfully applied for structure determination of metal complexes in solution. X-ray absorption spectroscopy (XAS) relies on the availability of strong X-ray

sources with continuous variation of the wavelength, as provided by synchrotron radiation. Most important is the spectral region of "extended X-ray absorption fine structure" (EXAFS) of XAS. Structural information is obtained from the interference pattern of the outgoing electron wave with the waves backscattered by the surrounding atoms. This information is limited to a sphere with a radius of about 5 Å around the metal. EXAFS yields distances between the central metal ion and the backscattering atoms, but only little information on directions. Therefore, it is frequently difficult or even impossible to unambiguously derive the structure of the complex from this limited information.

In this paper we will address this problem. We will describe a systematic approach which allows us to add further information from other sources and serves to arrive at a unique structure for metal–peptide complexes. Electron paramagnetic resonance (EPR) will be used to determine the nature of the atoms coordinating the metal; EXAFS spectroscopy as well as "electron spin echo envelope modulation" (ESEEM) will provide information on whether histidine residues of the peptide are taking part in the coordination. The positions of hydrogen atoms around the metal center will be obtained from "electron nuclear double resonance" (ENDOR). Chemical expertise on the structures and flexibilities of the peptide building blocks as well as of copper–peptide complexes will be added through a MM force field. Annealing strategies, like those commonly used in NMR, will be applied to combine all this information to enable a solution of the given optimization problem. The new method is applied to the Cu(II)-ligated octapeptide repeat sequence PHGGGWGQ of the human prion protein.

In the benign form the prion protein (PrP^C) is a GPI membrane-anchored protein with a large unstructured N-terminal tail containing four successive copies of the highly conserved octapeptide repeat sequence PHGGGWGQ, which was shown to bind up to four Cu^{2+} ions in a cooperative manner and at identical coordination geometries (Garnett and Viles 2003; Viles et al. 1999). There is ample evidence for the biological relevance of this copper binding, which ranges from a metal buffering role on the cell membrane surface to a copper transport function of the protein (Brown 2001a, 2001b; Lehmann 2002).

Structural analysis of the prion protein in solution revealed two domains: a globular C-terminal part (121–231) of PrP^C, as determined by NMR spectroscopy (Riek et al. 1997), and an unfolded N-terminal part, which is unstructured in the absence of bound Cu^{2+}. Since the presence of the paramagnetic Cu^{2+} ion limits standard NMR structural analysis, a variety of other techniques have been applied to characterize the structures of the Cu^{2+}-PrP^C complexes, particularly in the octarepeat region (Bonomo et al. 2000; Hasnain et al. 2001; Jackson et al. 2001; Viles et al. 1999; Whittal et al. 2000), including X-ray crystallographic analysis of a Cu^{2+} complex with HGGGW as the minimum binding unit (Burns et al. 2002). The crystal structure of the Cu^{2+}-HGGGW complex has clearly revealed a type II coordination geometry (Allen 2002), which involves three nitrogen ligands deriving from the His imidazole as well as from the deprotonated amides of the two adjacent Gly residues, and one oxygen ligand associated with the carbonyl group of the second Gly residue. An axial water completes the type II pentacoordination.

Spectroscopic investigations range from fluorescence (Hornshaw et al. 1995; Stöckel et al. 1998), UV-Vis (Miura et al. 1999), Raman (Miura et al. 1996, 1999) and CD (Aronoff-Spencer et al. 2000; Garnett and Viles 2003; Hornshaw et al. 1995; Luczkowski et al. 2002; Stöckel et al. 1998; Viles et al. 1999), through NMR (Luczkowski et al. 2002), to all kinds of EPR spectroscopy (Aronoff-Spencer et al. 2000; Cereghetti et al. 2001; Van Doorslaer et al. 2001): ENDOR, ESEEM (Burns et al. 2002; Van Doorslaer et al. 2001), 2DCP (Van Doorslaer et al. 2001) and HYSCORE (Burns et al. 2002; Van Doorslaer et al. 2001). However, despite substantial advances, the octarepeat-Cu^{2+} structure still remains a matter of debate, since some methods have yielded contradictory results. For instance, the copper complexation pattern significantly differs in the NMR (Luczkowski et al. 2002) and in the X-ray structures (Burns et al. 2002).

In part, the problems for structure determination originate from the strong effects of the environment such as pH and buffer composition. While the structural changes induced by the pH are well documented (Aronoff-Spencer et al. 2000; Cereghetti et al. 2001; Miura et al. 1999; Van Doorslaer et al. 2001), less attention has been paid to the role of the buffer in complex formation. Nevertheless, there are hints at the influence of the buffer, since Raman spectroscopy (Miura et al. 1996, 1999) indicates a hydrogen bond of the non-bonded imidazole nitrogen to a buffer molecule. Even the CD properties indicate significant effects of different buffers (Garnett and Viles 2003; Viles et al. 1999). Thus, differences of sample preparations have lead to strong variations in the experimental results and have hampered attempts to combine data from multiple sources into a single and consistent model structure. To exclude this source of uncertainty we have used in the present study a well-defined sample for application of a set of spectroscopic techniques which, combined with calculations using an MM force field, allowed us to generate a structural model which is consistent with all spectroscopic data.

Materials and methods

Unless stated otherwise, investigations were performed on 1 mM aqueous solutions of the octapeptide complexed with 1 equivalent of copper(II) (^{63}Cu for EPR and EXAFS). As buffer, 25 mM *N*-ethylmorpholine hydrochloride (NEM·HCl) and 150 mM KCl at pH 7.0 were used to ensure a 1:1 stoichiometry and high stability of

the peptide-Cu^{2+} complex. For low-temperature measurements, 20% glycerol was added. The synthesis and analytical characterization of the octapeptide Ac-PHGGGWGQ-NH_2 have been described elsewhere (Renner et al. 2004). The octapeptide corresponding to the sequence 60–67 of $hPrP^C$ was synthesized in the *N*-acetylated and *C*-amidated form, i.e. Ac-PHGGGWGQ-NH_2, to avoid end-group effects and, thus, to properly mimic this sequence portion in the intact protein. ^{63}CuO (Chemotrade) was stirred in 6 M HCl for 3 h at room temperature. Then the solution was filtered on 0.45 μm Millex-GV and the aqueous layer was lyophilized to yield $^{63}CuCl_2$ in quantitative amounts.

Isothermal titration calorimetry

Calorimetric isothermal titration (ITC) of the Cu^{2+}-octapeptide complex in 25 mM NEM·HCl/150 mM NaCl was carried out at 25 °C on a VP-ITC calorimeter (MicroCal, Northampton, Mass., USA) equipped with a 250-μL injection syringe. 100 μL of a 5 mM $CuCl_2$ solution containing 25 mM NEM·HCl/150 mM NaCl (pH 5.0) (20 injections, 5 μL per injection) were added under stirring (500 rpm), with 300 s spacing between injections. The filter period was 5 s, and no gain was used. The pH in the cell volume dropped during the titration from 7.5 to 7.0. However, in the unbound form, copper is not soluble at high pH and therefore the ligand solution in the syringe had to have a lower pH. The experimental data were fitted by using the single-set-of-identical-sites model built in the MicroCal Origin Software. As control experiments, titrations of copper to either NEM·HCl or phosphate buffer were performed.

Fluorescence

The emission spectra of Cu^{2+}/peptide mixtures at pH 7.2 and 25 °C ($\lambda_{ex} = 280$ nm, excitation and emission slits 3 nm, range 300–450 nm, scan speed 200 nm/min) were recorded with a Perkin-Elmer LS50B fluorimeter (Perkin-Elmer, Norwalk, Conn., USA) equipped with a RK 20 Lauda thermostat at 1.5×10^{-5} M peptide concentrations. A quartz cell with optical path of 0.2 cm was used and eight scans were accumulated. Copper induces quenching of the tryptophan fluorescence when bound to the peptide. Therefore, stoichiometry and approximate binding affinity could be obtained from a titration of the peptide with $CuCl_2$.

CD spectroscopy

CD spectra were recorded on a Jasco 715 spectropolarimeter (Jasco, Tokyo, Japan) provided with a PFD-350S temperature controller at peptide concentrations of 3×10^{-5} M to 3×10^{-4} M with quartz cells of 1 cm path length (Hellma, Baden, Germany). The spectra were registered in the 190–400 nm and 400–800 nm ranges at 0.1 nm resolution, 1 s response, 1 nm band width; 10 scans were accumulated to improve the signal-to-noise ratio and a scanning speed of 50–100 nm/min was applied.

NMR spectroscopy

NMR measurements were performed at 500 MHz with a DRX500 (Bruker Biospin, Karlsruhe) at 277 K. Samples contained between 0.1 and 2.0 mM peptide and between 0 and 25 mM NEM, and the pH was adjusted to 7.0 with small amounts of HCl or NaOH. One equivalent of $CuCl_2$ was used for preparation of the peptide-Cu^{2+} complex. Copper binding of NEM was tested using Cu^{2+}/NEM ratios between 1:50 and 9:1.

EXAFS experiments

EXAFS experiments were carried out at the Deutsches Elektronen-Synchrotron (DESY) in Hamburg, Germany, at the beamline D2 of EMBL. The storage ring DORIS was running at an energy of 4.4 GeV with a positron current between 80 and 150 mA. During the experiments the sample was kept at about 35 K within a closed-cycle helium cryostat. A Si(111) double monochromator with focusing mirrors selected an energy around the Cu K-edge, varying from 8700 to 9800 eV, corresponding to wave vectors k from 3.5 to 11 $Å^{-1}$. Seven Bragg reflections of a Si crystal detected by two scintillation counters were used for the energy calibration of the X-ray-beam (Pettifer and Hermes 1985). The K_α fluorescence was counted by a Canberra 13-element fluorescence detector. One scan took between 30 and 45 min. After each scan, the spectra of all detector channels were checked separately and individual channels showing parasitic resonances were excluded; the remaining channels were summed. Data were collected until the total number of fluorescence counts above the absorption edge accumulated to one million.

The EXAFS data were treated by standard procedures used at the EMBL outstation Hamburg (Nolting and Hermes 1992). Below the absorption edge the raw data were matched with a first-order polynomial. Above the edge the atomic absorption background was subtracted using a cubic spline fit with six knots. The k^3-weighted Cu EXAFS spectra $\chi(k)$ were refined with the software package EXCURV 9.262 (Binsted et al. 1992), using a least-squares refinement algorithm. Phase shifts and scattering amplitudes were computed according to Lee and Beni (1977).

EPR, ENDOR and ESEEM spectra

All spectra were recorded at X-band, 9.47 GHz, with a Bruker ELEXSYS 580 spectrometer. For continuous

wave measurements, the spectrometer was equipped with an Oxford cryostat with a variable-temperature control. ESR spectra were taken at 77 K with a modulation amplitude of 2 G and a microwave power of 0.2001 mW in a T_{102} Bruker cavity. For the simulation of the ESR spectra, the program package Xemr was used (compare: http://epr.chem.jyu.fi/xemr/). ENDOR spectra were recorded at 17 K with a microwave power of 20.0195 mW, a radiofrequency power of 2 dB at a maximum power output of 500 W and radiofrequency modulation amplitude of 300 kHz. Nine different ENDOR working points were chosen. ESEEM spectra were recorded at 5 K using a two-pulse sequence of 112 ns–τ–224 ns–acquisition. A two-pulse sequence was chosen owing to the limited bandwidth and pulse channels of the spectrometer. The hyperfine couplings of the nuclei to the electron spin of the Cu cause a periodic modulation of the electron spin echo amplitude as a function of the pulse separation time. Fourier transformation of the spin echo amplitude from time-space into frequency-space results in a hyperfine spectrum analogous to a corresponding ENDOR spectrum. Compared with ENDOR, much smaller hyperfine interaction energies can be detected.

Computational methods for simulated annealing and density functional theory calculations

The MM program XPLOR and its standard simulated annealing protocols (Brünger 1992) were used for the molecular dynamics (MD) simulations, by which the structures of the peptide–copper complexes were determined. The interactions within the peptide were modeled by the CHARMM22 force field (MacKerell et al. 1998). The additionally required MM parameters for a copper center complexed by three nitrogen and one oxygen atom and isotropic hyperfine coupling constants A_{iso} were derived by density functional theory (DFT) calculations using the BP86 functional and the 6-31G* basis set provided by the program Gaussian 98 (Frisch et al. 1998).

Theory and data analysis

EXAFS

According to Sayers et al. (1971), an EXAFS spectrum $\chi(k)$ can be computed by:

$$\chi(k) = \sum_{j=1}^{J} S_0^2 \frac{|f_j(k)|}{kR_j^2} \sin\left(\Phi + 2\delta_C + 2kR_j\right) e^{-2R_j/\lambda(k)} e^{-2\sigma_j^2 k^2} \quad (1)$$

The energy of the incoming X-rays is measured by the wave vector k. There are J non-hydrogen atoms, which contribute to the backscattering with amplitudes $f(k) = |f(k)|e^{i\phi(k)}$ at distances R_j from the central metal ion. δ_C is the central-atom partial-wave phase shift of the final state and $\lambda(k)$ the energy-dependent EXAFS mean free path. The thermal fluctuations of the distances are measured by the mean square displacements σ_j^2. This variable can also account for a distribution of molecular structures in the sample. S_0^2 is an overall amplitude factor, which is 0.9 in case of copper. Equation (1) refers only to single-scattering contributions. However, in the final step, multiple scattering processes are also considered up to the fifth order (Fonda 1992; Rehr and Albers 1990). Frequently, the least-squares fits of the spectra, in which the free parameters are the distances R_j, are performed by combining atoms at the same distances R_j into "shells" with N_R atoms. In our case, we did not proceed in this way but used a separate shell for each atom. This became possible because we had additional information on atomic positions from XPLOR. The σ_j^2 were optimized afterwards by hand.

EPR/ENDOR spectra

For the following explanation of our spectra analysis we introduce appropriate coordinates for the system under investigation (Fig. 1). A plane is defined containing the four ligands of Cu as good as possible. The Cu atom lies on the normal of this plane, which is called the z-axis. A rotation in the plane is described by the angle ϕ. A neighboring atom X (H or N) is at the position $2r$, rotated by the angle α with respect to z. The magnetic field $2B$ of the EPR spectrometer forms an angle θ with the z-axis of the molecular coordinate system.

The energy of the ^{63}Cu spin ($S = 1/2$, nuclear spin $I = 3/2$) is well described by the Hamiltonian:

$$\hat{H} = \beta_e \hat{S} g B + \hat{S} A_{Cu} \hat{I}_{Cu} \quad (2)$$

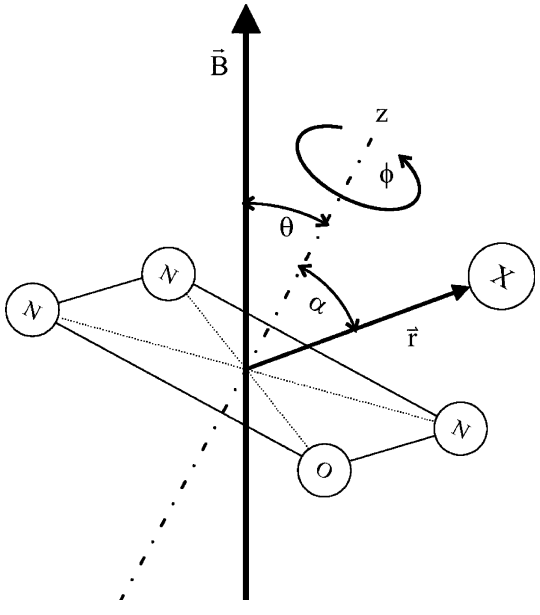

Fig. 1 The geometry for the ENDOR experiments

taking into account the electron Zeeman interaction and the nuclear hyperfine interaction. β_e is the Bohr magneton, $\hat{S}$ and $\hat{I}_{Cu}$ are the electron and nuclear spin operators, respectively. The $2g$ tensor and the magnetic hyperfine tensor, $2A$, are defined as usual.

ENDOR is sensitive to the nuclear spins of one or more atoms X up to 5 Å distant from the Cu ($I=1/2$ for $X={}^{1}H$ and $I=1$ for $X={}^{14}N$). A resonant radiofrequency is a measure of the hyperfine splitting due to the neighboring atoms X. This interaction cannot be resolved by EPR. It is described by the following Hamiltonian:

$$\hat{H}_X = g_N\beta_N B\hat{I}_X + \hat{S}A_X^{Dipole}\hat{I}_X + \hat{S}A_X^{Fermi}\hat{I}_X \quad (3)$$

The first term gives the nuclear Zeeman energy. The hyperfine interactions with the electron spin S of the Cu atom are described by the second and third terms. We have:

$$A_{ij}^{Dipole} = \frac{-\beta g_N\beta_N}{h|r|^3} g_i\left(3r_i r_j - \delta_{ij}\right) \quad (4)$$

and:

$$A_{ij}^{Fermi} = A_{iso}\delta_{ij} \quad (5)$$

In principle, a nuclear quadrupole interaction should be added in Eq. (3). Since we did not use it in our evaluations, we omitted it.

Here, g_N is the nuclear g-factor and β_N is the nuclear magneton. The nuclear spin operator is represented by $\hat{I}_X$. Two magnetic hyperfine tensors describe the interaction of the nucleus X with the spin S of the Cu. A^{Fermi} is the Fermi interaction matrix where A_{iso} is the isotropic Fermi interaction, and δ_{ij} the Kronecker symbol. A^{Dipole} gives the dipole–dipole interaction matrix. While the **g**-tensor becomes diagonal in the chosen coordinate system, the **A**-tensor may not be diagonal in this system.

For protons, the nuclear Zeeman effect dominates. Therefore, ENDOR lines occur centered at the nuclear Zeeman frequency, which is about 12–14 MHz, depending on the magnetic field. The lines are split by the magnetic dipole–dipole hyperfine and the Fermi-contact interactions. The other terms can be neglected. In the case of ^{14}N, the dominating term is the Fermi interaction; the dipole–dipole interaction can be neglected. In a frozen solution the z-axis is randomly oriented with respect to $2B$. Choosing a specific B-value, which is equivalent to the choice of a $g(\theta,\phi)$-value, selects those molecules for EPR excitation and hence for the ENDOR experiment which have the angle θ between their z-axis and $2B$. Since only the angle θ is selected, the experiments average over the angle ϕ.

For the interpretation of the ENDOR data, a Maple (Maplesoft, Waterloo Maple) program had to be written. The Hamiltonian matrix was diagonalized to compute the transition energies. All transition energies were averaged over the angle distribution to generate the ENDOR spectrum for the frozen solution sample. Transition moments have not been calculated.

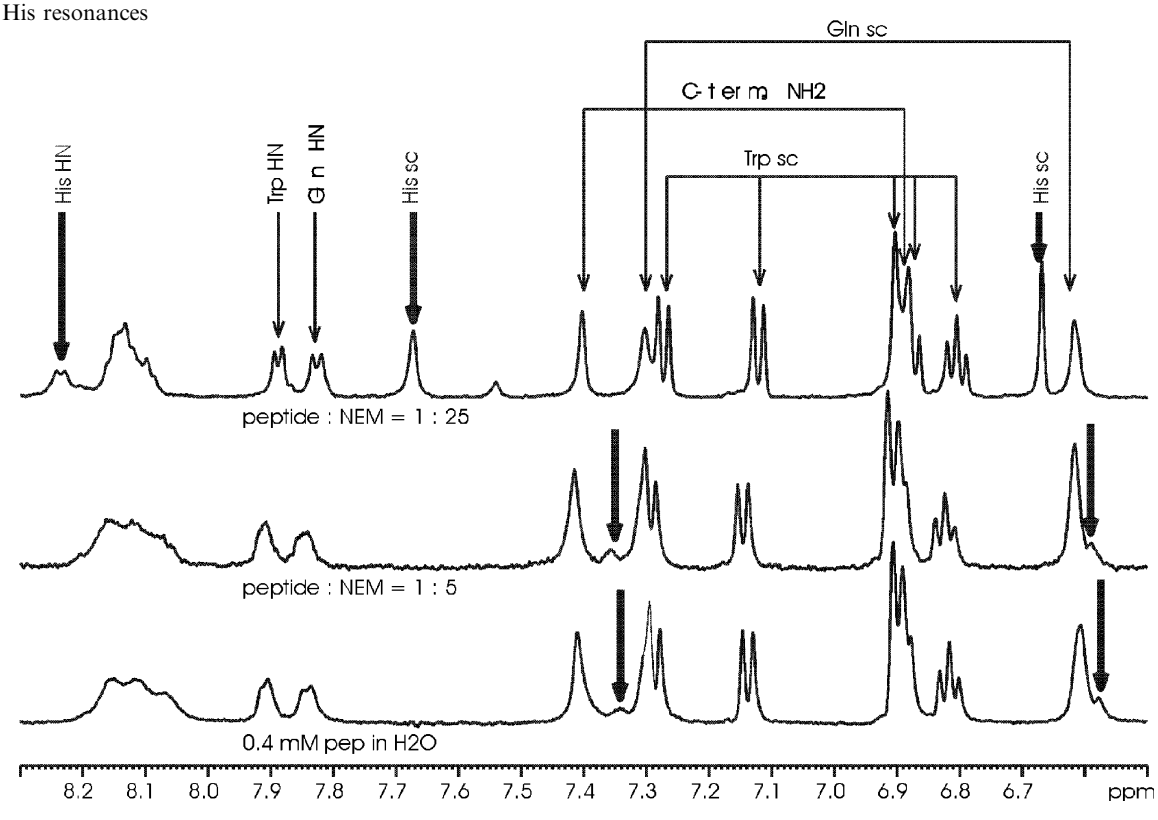

Fig. 2 1D ^{1}H NMR spectra of 0.4 mM peptide in water at pH 7.1 and 277 K with varying amounts of NEM. Assignment of NMR resonances is given above the spectra. *Bold arrows* indicate the varying His resonances

Results

Cu^{2+}-octapeptide complex formation in NEM buffer

Strong bands in the circular dichroism (CD) spectra in the visible range clearly showed the presence of a fully asymmetric coordination of the copper for the octapeptide-copper complex in NEM·HCl buffer, in agreement with spectra reported previously (Viles et al. 1999). In pure water the signal was weaker, suggesting a stabilizing role of NEM for the copper complex under investigation. Use of phosphate buffer even led to complete loss of the dichroic signal in the visible range, indicating competition of phosphate with the peptide for copper complexation. Isothermal calorimetric titrations of copper to either NEM·HCl or phosphate buffer confirmed that NEM does not interact detectably with copper, whereas phosphate exhibits an affinity to the metal that is on the same order of magnitude as that of the peptide. For the peptide dissolved in pure water, quenching of the tryptophan fluorescence occurs upon addition of $CuCl_2$. This collisional quenching of tryptophan by copper ions vanishes in the presence of NEM, again pointing to an influence of NEM on the peptide-metal complex.

In the isothermal calorimetric titration of copper to the octapeptide in NEM buffer, the best fitting of the titration points was obtained for a molar ratio of 1:1. The reaction is exothermic with a ΔH of -4.56 kJ/mol and a binding affinity of $K_a = 1.4\times10^5$ M ($K_d = 7.2\times10^{-6}$ M). This agrees well with previously determined affinities for

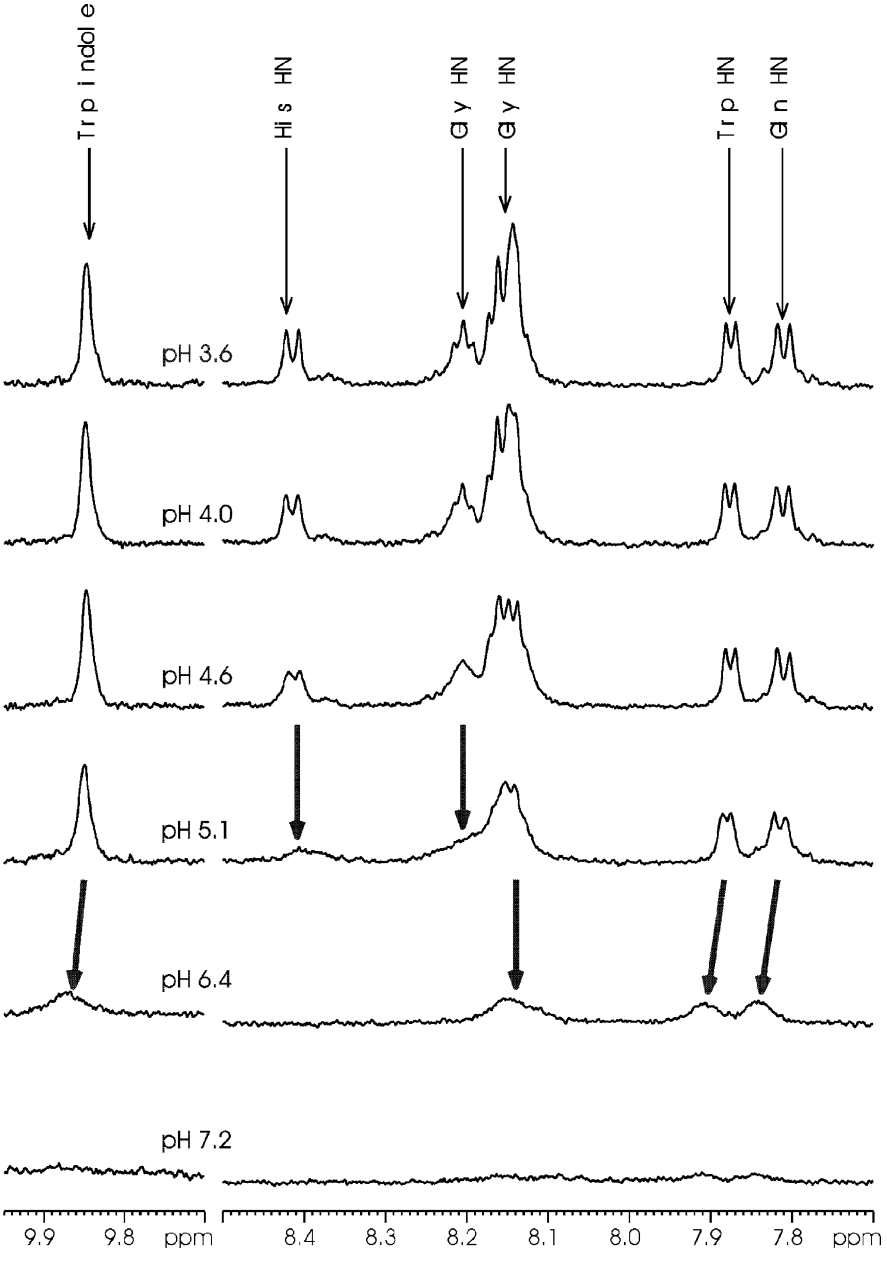

Fig. 3 1D ^{1}H NMR spectra of 0.25 mM octapeptide in 25 mM NEM/75 mM KCl at different pH values and at 277 K. Assignment of amide protons is given above the spectra. *Bold arrows* indicate significant changes in the spectra

the octarepeat region of PrP^{c}: 14 μM in MES buffer by fluorescence and equilibrium dialysis (Garnett and Viles 2003; Hornshaw et al. 1995; Kramer et al. 2001; Stöckel et al. 1998), 6.7 μM in phosphate buffered saline (PBS) by fluorescence (Garnett and Viles 2003; Hornshaw et al. 1995; Kramer et al. 2001; Stöckel et al. 1998) and 6 μM in water or NEM by CD (Garnett and Viles 2003; Hornshaw et al. 1995; Kramer et al. 2001; Stöckel et al. 1998).

NMR spectroscopy was used to clarify the role of NEM in the copper binding of the octapeptide. No indications of a direct NEM–Cu^{2+} interaction could be found from 1D ^{1}H NMR experiments, consistent with the calorimetric results. No change of the NMR resonances of NEM was observed even at high Cu^{2+}/NEM ratios, except for a general line broadening caused by the presence of a paramagnetic species in the solution. However, an influence of NEM on the histidine resonances of the octapeptide can clearly be seen in Fig. 2. Only at high NEM concentrations is strong line narrowing observed for the amide H_N as well as the side-chain protons of His, indicating a weak, but distinct, interaction between NEM and the octapeptide. The line narrowing effect can be explained by stabilization of the protonation state of the His side-chain at high NEM concentrations. The pH-dependent formation of the octapeptide-Cu^{2+} complex was monitored by NMR spectroscopy for a peptide/Cu^{2+} ratio of 1:1 and in the presence of NEM (Fig. 3). In a first step, the resonances of His and of one Gly disappear between pH 4.6 and 5.1, whereas the other NMR signals remain virtually unaffected. In a second step at higher pH, all peptide resonances are dramatically broadened. An unspecific effect of copper ions on the NMR spectrum can be ruled out, as buffer signals such as those originating from NEM experience only slight broadening even at high pH. Apparently, histidine is binding to Cu^{2+} already at pH 5.0, at which the rest of the peptide does not yet participate in complex formation. However, the stoichiometry of the peptide-Cu^{2+} complex at lower pH cannot be deduced from these measurements.

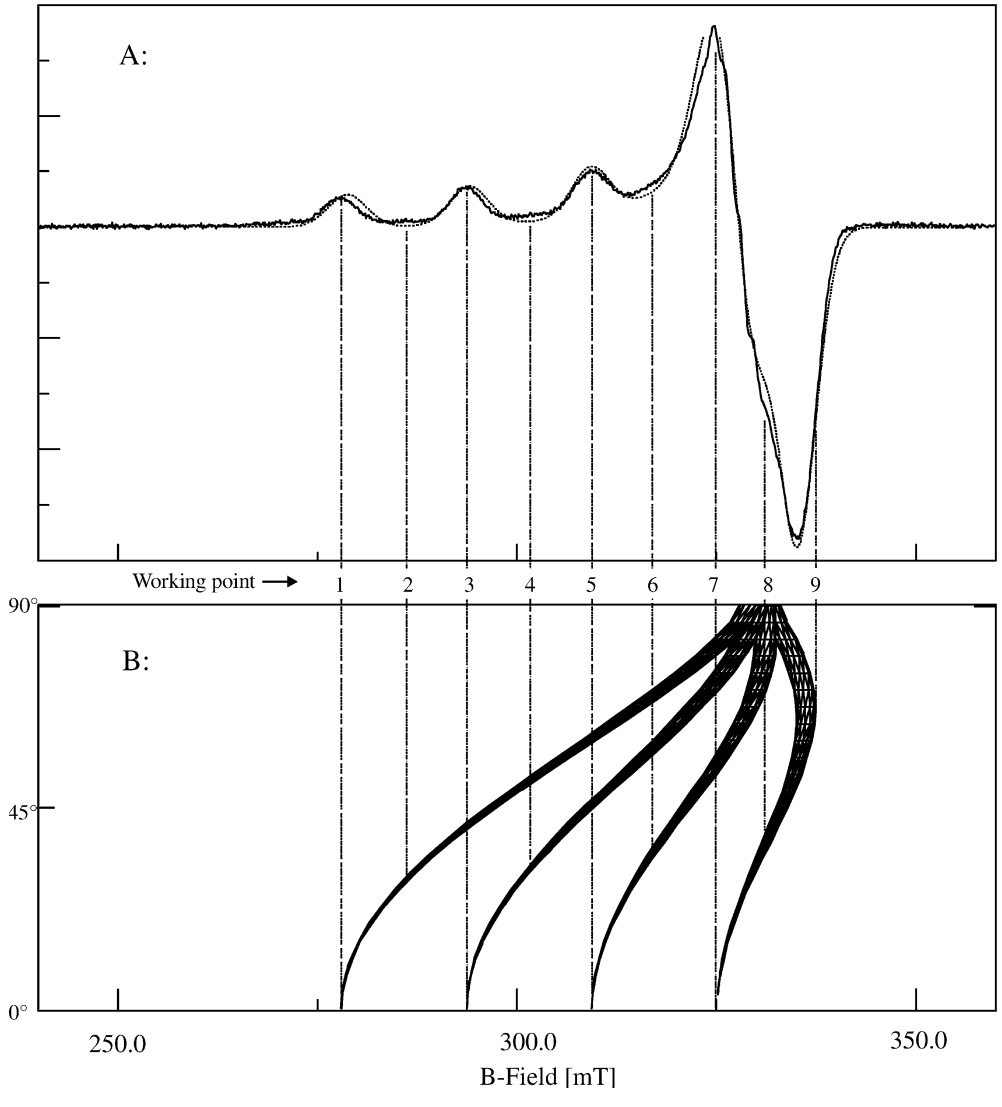

Fig. 4 **A** X-Band EPR spectrum of the prion octarepeat (*solid line*) and spectrum simulation (*dotted line*). The simulation parameters are $g(x) = 2.057$, $g(y) = 2.073$, $g(z) = 2.248$, $A(x) = 0.78$ mT, $A(y) = 0.78$ mT, $A(z) = 16.5$ mT, line width = 4.9 mT, Lorentz/Gauss = 0.26. The spectrum was recorded at 77 K, $\nu_0 = 9.492$ GHz. **B** The contribution of single ^{63}Cu nuclear sublevels to the EPR spectrum is displayed. The position of the nine ENDOR working points and therefore the fixation of ϕ is given

EPR spectra

Figure 4A depicts the hyperfine splitting of the EPR spectrum due to the interaction of the Cu(II) spin ($S = 1/2$) and the ^{63}Cu nucleus ($I = 3/2$). The EPR spectrum has been measured at 77 K. For the planar coordination pattern shown in Fig. 1, a good theoretical fit (dotted line in Fig. 4A) to the spectrum (solid line) has been achieved using the methods described above; the resulting fit parameters are given in the figure caption. The relatively small line widths and the good agreement with the simulated spectrum lead to the conclusion that the sample contains only one species. According to Peisach–Blumberg correlations (Peisach and Blumberg 1974), this spectrum is compatible with three nitrogen and one oxygen ligands in the equatorial plane. However, weak five- or six-fold coordination along the z-axis cannot be excluded. The dependence of the EPR resonances on the orientation of the molecules relative to the direction of the magnetic field is shown in Fig. 4B. Molecules with a z-axis parallel to B have four well-separated resonances; in molecules with z perpendicular to B_0, the signals collapse at $B = 328.3$ mT.

ESEEM spectra

The lines marked in Fig. 5 are caused by one weakly coupled ^{14}N. If one assumes that an imidazole is bound to the copper ion, these lines originate from the non-bonded nitrogen of the imidazole ring.

EXAFS spectra

The spectrum of the Cu^{2+}-peptide complex is shown in Fig. 6. In the first instance the experimental results were analyzed with a simple model, in which three N atoms and one O atom are assumed to coordinate the Cu^{2+}. One of these N atoms belongs to the imidazole ring of a His, which is included in this "basic model". This is clearly seen from the two peaks between 2.5 and 4.5 Å in the Fourier transform of the spectrum (Fig. 6B) (Arnesano et al. 2003b; Hasnain et al. 2001; Meneghini and Morante 1998; Steiner et al. 2002). The following distances have been determined by a least-squares fit: N–Cu, 1.95 Å (×2); N_δ–Cu, 1.91 Å; O(carbonyl)–Cu, 2.00 Å; and O(water)–Cu, 2.35 Å. Because EXAFS yields distances, each coordinating atom has to be located on a sphere with a radius given by the corresponding distance from the metal ion. In the calculation for the basic model, multiple scattering was taken into account only for the imidazole group. This allowed us to determine the angle between the copper atom and the two imidazole nitrogens. It is obvious that the fit does not explain the experimental results sufficiently well. We will show later how a satisfactory fit of the data (Fig. 6B) can be obtained.

ENDOR spectra

Spectra were recorded at the nine different ESR working points, as indicated in Fig. 4. Table 1 shows the orientations of the selected molecules. The corresponding ENDOR spectra are depicted in Fig. 7. The ENDOR spectra show ^{1}H resonances in the region of 9–17 MHz, which appear symmetrically around the proton nuclear Zeeman frequency of 12–14 MHz. Apart from the Cu^{2+}–proton geometry determining A_{dipole}, the ^{1}H ENDOR spectra are also influenced by the isotropic hyperfine interaction A_{iso}. Because the hyperfine inter-

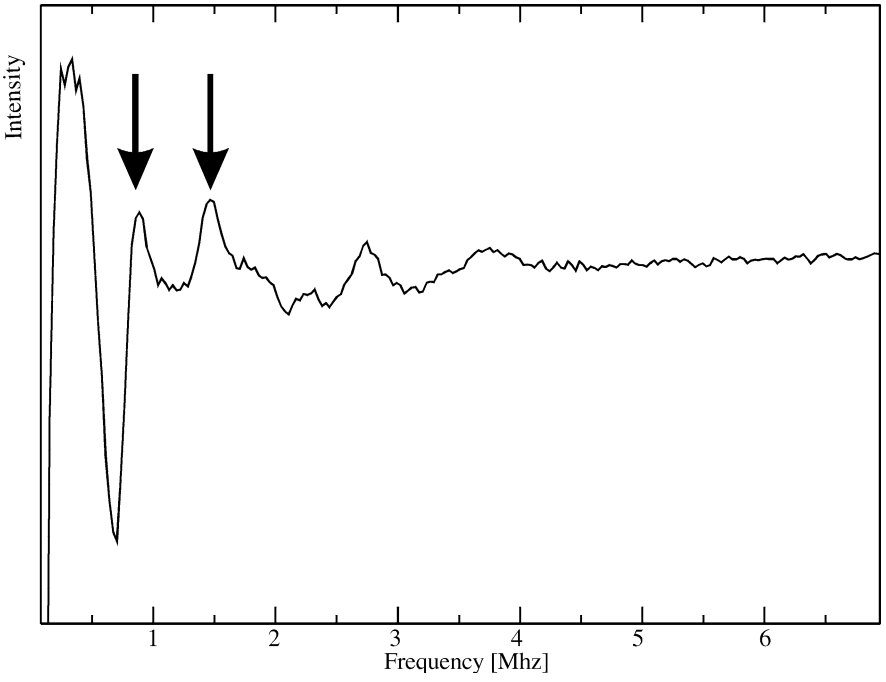

Fig. 5 X-Band two-pulse ESEEM spectrum of the prion octarepeat. The spectrum was obtained from the $g_\perp = 2.248$ region at 5 K. The lines at 0.8 and 1.5 MHz (marked with *arrows*) indicate a weakly coupled ^{14}N

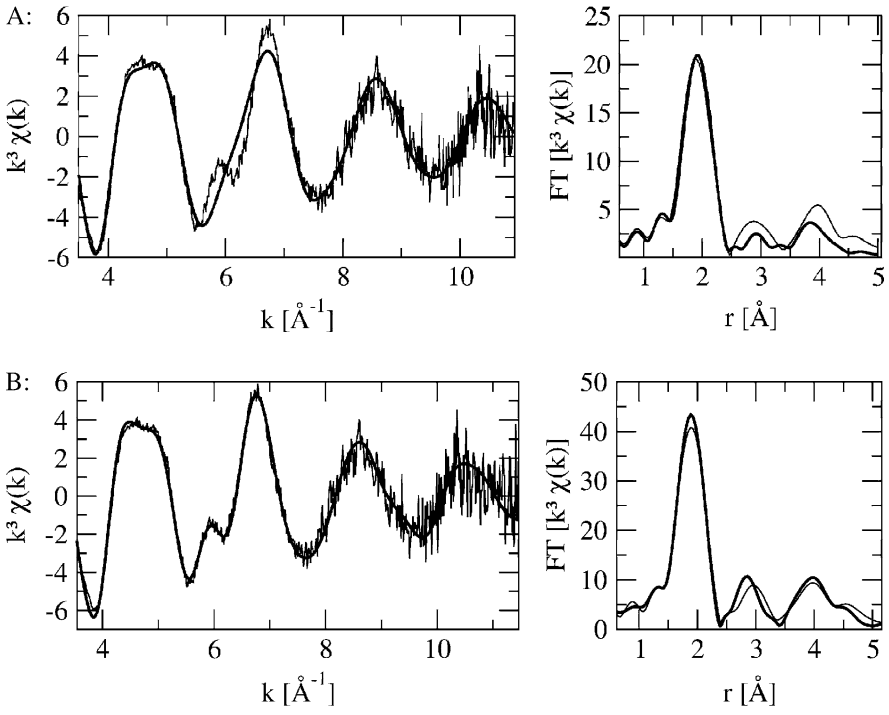

Fig. 6 EXAFS spectrum and its Fourier transform of (**A**) the basic model and (**B**) the final model. *Solid line*: experimental data; *dashed line*: calculated from structural model

action consists of the sum of the dipolar and the isotropic interactions, the knowledge of the magnitude of the isotropic interaction is crucial for the interpretation of the proton ENDOR spectra. Concerning copper complexes, reliable literature data are available for histidine ligands. As the most frequent copper ligand, histidine has been a matter of interest in the past. Many of the isotropic interaction parameters have been assigned in the course of paramagnetic NMR studies. Conversely, for other ligands, data are not available. For σ-bound ligands, and mainly based on Ni complexes, the Karplus relation (Pardi et al. 1984) has been established. However, for copper complexes, no detailed investigation has been reported so far. Therefore, DFT calculations have been performed in order to estimate the magnitude of the isotropic hyperfine interaction concerning the backbone copper ligands.

An additional set of lines appear in the low-frequency region (5–9 MHz), which is shown in Fig. 7. They are most clearly visible in the spectrum at working point 1.

Table 1 The magnetic field and the selected angles θ for each ENDOR working point

Working point	Magnetic field (T)	Selected angles θ (°)
1	0.2790	0
2	0.2864	27
3	0.2938	0, 40
4	0.3010	31, 50
5	0.3082	0, 45, 59
6	0.3156	35, 68, 69
7	0.3230	0, 54, 72, 80
8	0.3283	34, 70, 90
9	0.3340	66

Therefore, the four lines were assigned to two backbone ^{14}N ligands. Especially in the spectrum at working point 1, there are also lines visible in the high-frequency region (15–20 MHz). This set of lines appears in a frequency region that is known to contain lines of ^{14}N ligands of imidazole rings. However, the statistics were too poor to allow clear assignment of all four lines in all ENDOR spectra; moreover, the lines were found to overlap partly with ^{1}H ENDOR lines.

The spectra shown in Fig. 7 were used to determine possible H-positions, which are listed in Table 2 assuming $A_{iso} = 0$. For an estimated position $2r$ for a proton, the corresponding ENDOR spectrum was calculated. This position is a valid H position, if the calculated signals are found in all nine experimental ENDOR spectra. The contributions of different protons are then added. Table 2 gives the result of these calculations. This preliminary interpretation of the ENDOR data was then systematically refined in conjunction with the other experimental and computational data, as described in the next section.

In Fig. 8, ENDOR spectra of samples in H_2O and D_2O solutions are compared at working points 1 and 8. One difference between the H_2O and the D_2O spectra is seen at the central line, which is smaller for all D_2O ENDOR spectra owing to missing protons at high distances from the Cu center. Whereas the ENDOR spectra of D_2O and H_2O at working point 8, reflecting planar protons only (Hurst et al. 1985), show no substantial difference, there is a significant difference in the spectra of working point 1, which shows solely protons at the axial position (Fig. 8). Since there are no exchangeable protons of the peptide backbone in appropriate positions, the missing resonance lines in Fig. 8 can be

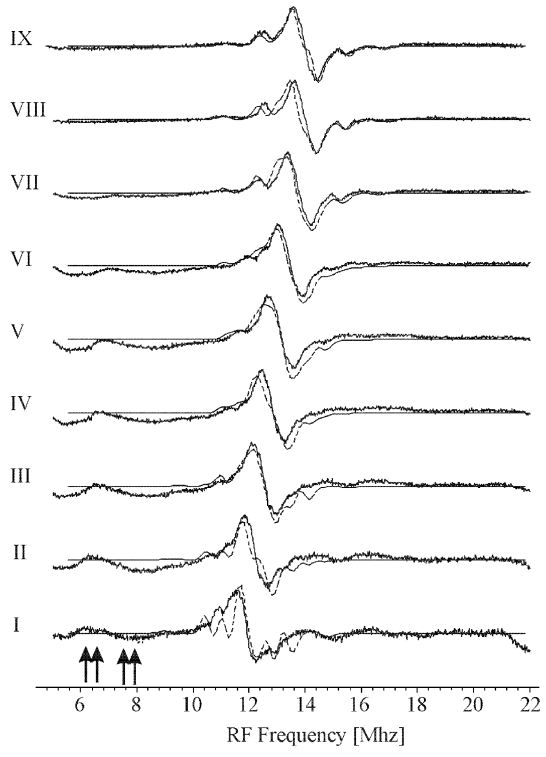

Fig. 7 ENDOR spectra for all nine ENDOR working points (*solid line*) and simulation of these ENDOR spectra (*dashed line*). One set of protons has to match all nine experimental spectra at once

Table 2 Proton distances from Cu. The angle θ refers to an axis perpendicular to the 3N-1O plane. The method is insensitive for distances larger 5 Å

Cu–H distance (Å)	θ(°)
3.1	60
3.0–3.1	90
3.9–3.95	60
3.85 – 3.9	40–60
4.75	30

unambiguously assigned to protons from a water molecule which is coordinating the Cu center in an axial position. Protons of the histidine appear at working point 8 (Fig. 8).

MM force field for simulated annealing calculations of peptide-copper complexes

Since CHARMM22 provides a MM force field solely for standard components of peptides and proteins (MacKerell et al. 1998), a set of MM parameters was required for the octarepeat copper complex. To estimate such parameters we have scanned the potential energy surface of the model compound depicted in Fig. 9a by DFT calculations. The choice of this model compound has been motivated by the following considerations. The imidazole ring serves to model a histidine residue; the HN–COH and H_2N–COH groups represent amide groups of a peptide bound to Cu^{2+} through N and carbonyl O atoms, respectively. Minimal models have been chosen for all ligands so as to avoid mutual contacts. It should be emphasized that the Cu ligation to one O and three N, with one N belonging to a histidine, is not questionable. Therefore, the model in Fig. 9a is general enough. The force field parameters resulting from least-square fits of the MM to the DFT potential surface are collected in Table 3 and are explained in the caption. Note, in particular, that the harmonic dihedral potentials are quite flat, as indicated by the rather small k_δ values of 54 kJ/(mol rad) and weakly favor a planar geometry of the copper complex, as shown by the equilibrium δ_0 values at 180°. Details will be published elsewhere (A. Weiss and P. Tavan, in preparation).

DFT calculation of the isotropic hyperfine interaction

According to Eq. (3), the simulation of the ENDOR spectra requires appropriate values of the isotropic hyperfine coupling constant A_{iso} appearing in Eq. (5). In the given case of a Cu^{2+} complex involving a histidine, two amide nitrogens and one carbonyl oxygen, the molecular model depicted in Fig. 9b should represent the chemical environment of the Cu^{2+} reasonably well (see above) and, therefore, has been used for DFT calculations of A_{iso} employing the methods described above. The dominant contributions to A_{iso} are due to Fermi contact couplings between the electron spin of the Cu^{2+} and the nuclear spins of those hydrogen atoms that are covalently connected through intermediate nitrogen and carbon atoms. In particular a proton H′, which is attached to the C_α atom of a glycine residue coordinating the Cu^{2+} through its amide nitrogen, can contribute to A_{iso} in a geometry-dependent manner. The corresponding Fermi contact couplings sensitively depend on the Cu^{2+}–N–C_α–H′ dihedral angle δ (see Fig. 9b for a sketch of this geometric parameter in the model compound). Figure 9 shows the DFT results (dots) on the δ dependence of A_{iso} for the coupling of a single proton H′ to the copper. In addition, it contains a fit of the model $A_{iso}(\delta) = c\sin^2(\delta - \delta_0)$, with the parameters $c = 9.7$ G and $\delta_0 = -27°$.

Structure determination by combining EXAFS, EPR, ENDOR, ESEEM and MD simulated annealing

In this section, we present a new approach to obtain structural information by a systematic combination of different spectroscopic experiments with simulated annealing on the computer. The EPR spectrum of the Cu(II)-ligated octapeptide indicates a coordination of the metal ion with three nitrogen atoms and one oxygen atom in a nearly planar geometry. From the sequence of the peptide, the following atoms are to be considered as potential candidates: the two nitrogens of the His resi-

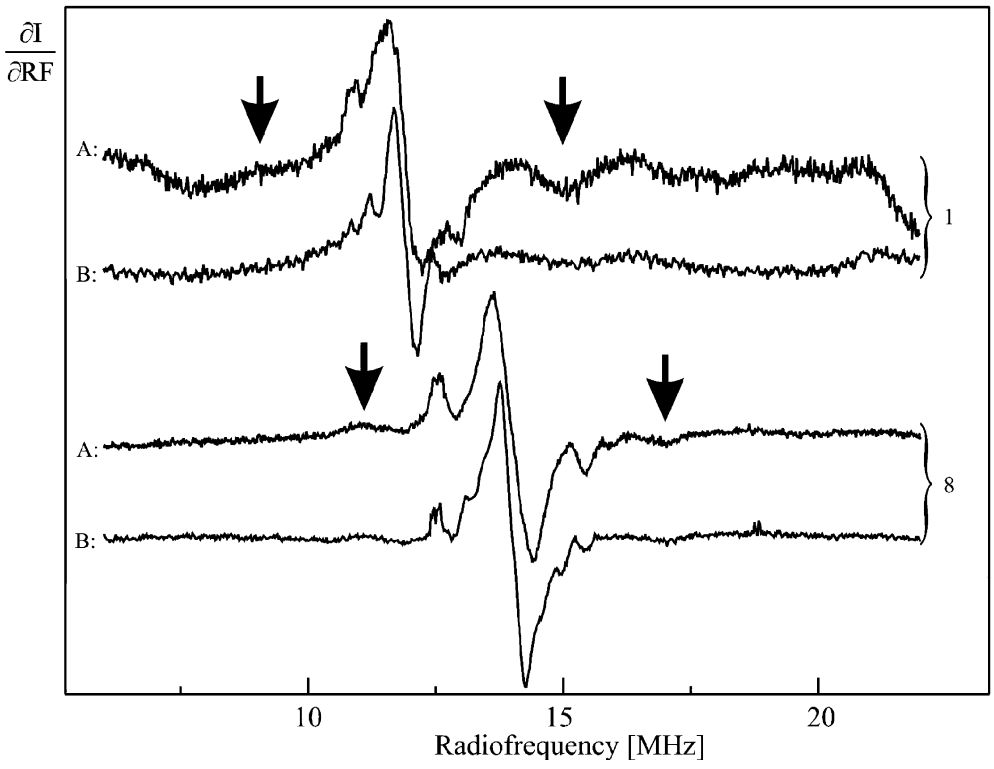

Fig. 8 Comparison of ENDOR spectra of the octapeptide-Cu complex in H_2O (**A**) and D_2O (**B**) solutions for the working points 1 and 8. At the working point 1 the *arrows* indicate the resonances which are assigned to the axial water ligand. At the working point 8 the resonances attributed to an H of the histidine are marked by *arrows*

due, the eight amide nitrogens and eight carbonyl oxygens. ^{14}N ENDOR and ESEEM results show that one nitrogen of an imidazole coordinates the Cu^{2+}. Although Miura et al. (1996, 1999) suggest that the N_δ of the imidazole ring is bound to the copper, our computational approach was not restricted by this finding

Fig. 9 Isotropic Fermi contact couplings A_{iso} as a function of the Cu–N–C_α–H′ dihedral angle δ as calculated by DFT (*black dots*) from the model compound (*b*) shown on right. The *solid line* is the fit described in the text. Model (*a*) was used to calculate the MM force field parameters listed in Table 3. For explanations, see the text

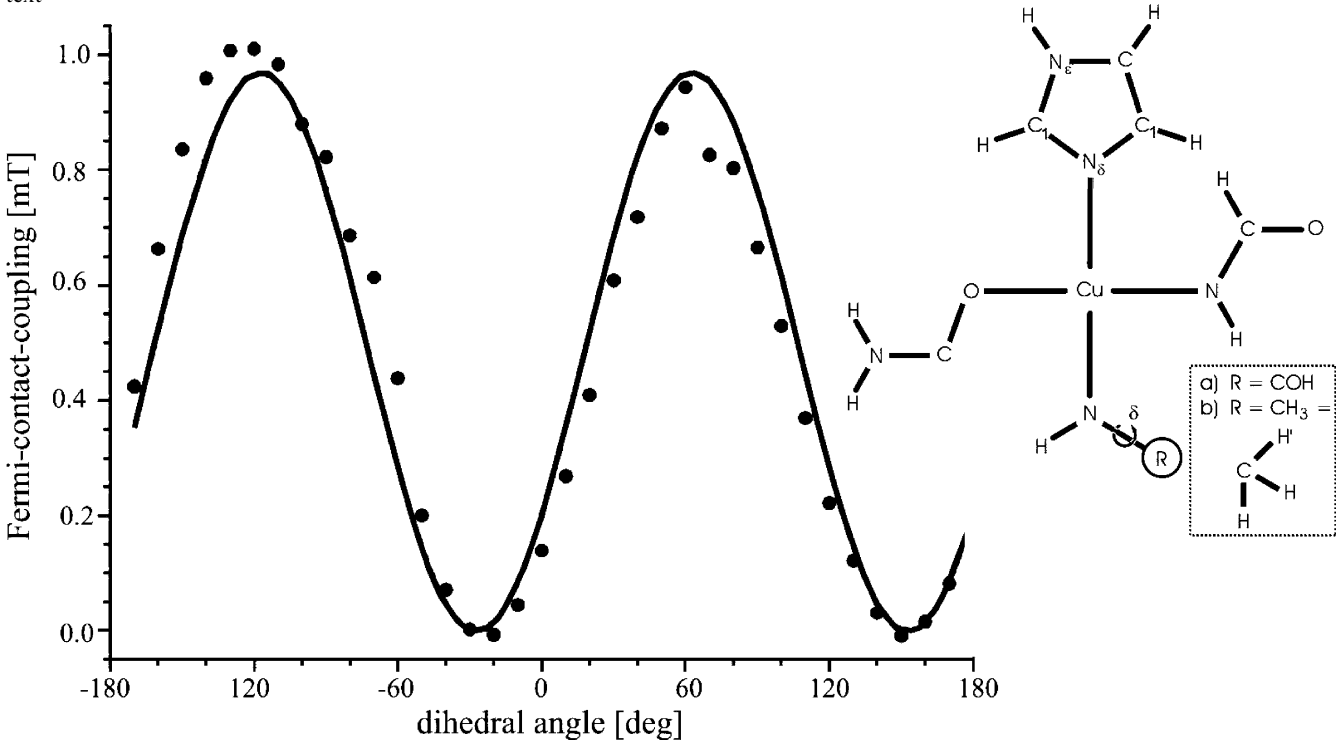

Table 3 Force field parameters of a five-fold coordinated Cu^{2+} center derived from DFT calculations on the model compound shown in Fig. 9a. As is common in the CHARMM22 force field (MacKerell et al. 1998), the bond lengths l and angles$\gamma$are modeled by harmonic potentials characterized by equilibrium values l_0 andγ_0 as well as by force constants k_l and k_γ, respectively. In addition, four harmonic dihedral potentials serve to stabilize the planarity of the Cu^{2+}coordination by one oxygen and three nitrogen atoms. Here, $N_\delta$is the nitrogen of the imidazole ring. Planarity is achieved by choosing equilibrium valuesδ_0 and force constants k_δ for the dihedral angles δ defined in the usual way by the sequence of atoms X–Cu–Y–Z, where X,Y,Z are chosen from the set of coordinating atoms {N_δ,N,O}. The electrostatics is covered by partial charges optimally reproducing the electrostatic potential near the van der Waals surface of the molecule, i.e. by the so-called ESP charges computed by GAUSSIAN 98 (Frisch et al. 1998). The parameters of the Cu Lennard-Jones (LJ) potential have been adopted from the work of Comba and Remenyi (2002)

Bond lengths	l_0 (Å)	k_l [kJ/(mol Å)]
Cu–N_δ	2.01	540
Cu–N	1.98	750
Cu–O	2.09	190
Cu–H_2O	2.34	210
Bond angles	γ_0(°)	k_γ [kJ/(mol rad)]
C_1–N–Cu	134	230
C_1–N_δ–Cu	114	230
C–N–Cu	120	230
C–O–Cu	120	230
Dihedral angles	δ_0(°)	k_δ [kJ/(mol rad)]
X–Cu–Y–Z	180	54
Partial charges	q(e)	
Cu	1.08	
O	−0.51	
N	−0.7	
N_δ	−0.7	
LJ parameters	σ(Å)	ϵ(kJ/mol)
Cu	1.2	0.21

and both, so N_δ and N_ϵ are considered as possible ligation atoms. Taking into account all the possible remaining nitrogen and oxygen atoms, there are 378 different possibilities, i.e. configurations, for the copper complexation.

In a first step, 378 starting structures for subsequent MM energy refinement have been generated. This process was repeated 12 times for each configuration. For this purpose, first an extended random coil structure was assumed for the peptide and the metal ion was covalently attached to the N_δ and N_ϵ atoms, respectively, of the histidine. Since measurements of a deuterated sample revealed exchangeable protons in an axial position, a water molecule was positioned as a weak axial ligand. To obtain an energetically relaxed structure, an initial simulated annealing protocol involving cooling from 3000 K to 0 K was applied to the random-coil peptide using the MM-MD program XPLOR (Brünger et al. 1987). In this initial annealing simulation the complete CHARMM22 force field (including the standard partial charges for the peptide and a charge of +2e for the Cu) was employed. To generate a sample structure for one of the 378 different ligation patterns, the respective amide nitrogens were deprotonated and negatively charged, and during a subsequent 150 ps annealing simulation the ionic interaction between the selected amide nitrogens and the copper was slowly replaced by harmonic distance restraints serving to model a covalent coordination of the Cu. Simultaneously, the negative charges of the amide nitrogens (−1.16e) and the positive charge (+2e) of the Cu ion were reduced towards the values of −0.70e and 1.08e, respectively, which correspond to the standard values in our MM force field for such Cu complexes (cf. Table 3).

The 12×378 configurations generated in this way were the starting points for the further refinements. The complete MM force field for such copper complexes, including potentials for bond stretches, angular deformations, and torsions around bonds, has been used in subsequent standard simulated annealing procedures (Brünger et al. 1987). 1200 annealing runs have been executed for each starting structure, resulting in a total of 453,600 different peptide-Cu structures.

To remove all structures which were completely incompatible with the experimental data or with the force field, we applied the following selection rules. The effectiveness of these rules is summarized in Table 4. (1) Only structures that had copper–ligand distances in the interval 1.85–2.1 Å [and (2) with no other atoms closer than 2.3 Å to the copper center], were accepted. (3) The near planarity of the copper–ligand coordination was ensured by selecting only structures in which no ligand atoms deviated by more than 10° from planarity. (4) For a ligation of N_δ to the copper, the results of EXAFS experiments demanded structures with a Cu^{2+}–N_δ–C angle in the range between 150° and 165°. For a ligation of N_ϵ, we did not apply this selection rule. These requirements had to be met by all structures (“global criteria”). Two further criteria have been applied to select the best structures within each of the 378 binding motifs m (“local criteria”). (5) For each m the average $< E_m >$ of the total energy E_m was calculated and only structures with $E_m < < E_m >$ were selected. (6) Deviations of geometric parameters (bond lengths, angles, dihedral angles) from their respective equilibrium values as given by the peptide force field were collected into a least-squares deviations scoring function. Only structures with scores better than the average score within the respective class m were selected and with no bonds, angles or dihedrals violating the equilibrium structure given by the force field.

For thus-obtained structures, EXAFS spectra were calculated. In these calculations, multiple scattering was taken into account, with up to four scattering processes. Multiple scattering strongly depends on the atoms within the second and third coordination spheres around the copper and not on the direct ligands. Therefore, each modification of the peptide conformation results in large changes of the EXAFS multiple scattering contributions, which in many cases are incompatible with the observations. This incompatibility excludes all configurations with N_ϵ ligation (11) and another 13 of the 19 binding motifs with N_δ ligation, leaving six configurations as possible candidates. For each of these six con-

figurations, 500 simulated annealing calculations have been performed. By using our MM force field for the copper complex in our final combinatorial approach, we found that the variation of the equilibrium distances of the first ligands is high (1.5 Å < r < 2.5 Å). Since the experimentally determined EXAFS distances are more precise than the MM parameters derived from the DFT calculations on small model compounds, they were used in the MM force field for generation of a more accurate structural model.

In the next step we have used the information of hydrogen positions as obtained by ENDOR. The experiments yield the hyperfine interactions of all H-atoms in a sphere with a radius of 5 Å around the Cu. For the 3000 structures obtained in the preceding step, the positions of the hydrogen atoms are known and the hyperfine interactions were calculated. In three structural motifs m, calculation yielded resonances that are not observed by ENDOR. For the remaining 1500 structures, EXAFS spectra have been re-calculated and compared with the experiments. For each motif, one structure was selected that best fitted the experimental data. Then, the resulting structures were refined by changing the Debye–Waller factors of the atoms, whereas changes in the ligand distances were not required. The best result for reproducing the EXAFS data is shown in Fig. 6B and the corresponding structure of the Cu^{2+}-octapeptide complex is displayed in Fig. 10. In the rejected configurations the N or the N and the carbonyl O of Trp6 are ligands of the copper. In both cases the structure did not allow us to reproduce the EXAFS experiments in the region of $k \approx 6$ Å^{-1}.

Discussion

Studies on the Cu^{2+} complexation by PrP and related peptides have been performed in various buffers such as Tris·HCl, NEM·HCl, phosphate and acetate (Garnett and Viles 2003; Viles et al. 1999). Among these, mainly NEM buffer was used, since Tris was reported to compete efficiently for Cu^{2+} (Viles et al. 1999). PBS is largely used in biological studies to mimic physiological fluids. Correspondingly, NEM and phosphate buffer were comparatively analysed for their compatibility with copper binding to the PrP peptide. Phosphate seems to compete with the octapeptide for copper complexation and was therefore discarded. Also, EPR spectra of the octarepeat in phosphate buffer and NEM differed significantly. Clearly, the influence of the buffer on the result of spectroscopic measurements is large. Because of its apparently stabilizing action and for easier comparison with literature data, we chose NEM buffer for our investigations. Moreover, to mimic physiological conditions, a pH value of 7 was used.

The atom types of the first ligands have been determined by peptide fragment experiments (Aronoff-Spencer et al. 2000; Miura et al. 1999). For a pH value of 7.4 there is little doubt that the dominant species of copper complexation is 3N and 1O. According to the Peisach–Blumberg correlations (Aronoff-Spencer et al. 2000; Peisach and Blumberg 1974), the fitted EPR parameters of the Cu^{2+}-octapeptide complex are consistent with a ligation by three nitrogen and one oxygen atoms in a planar configuration. For the structure determination, the planarity of the complex was used as the boundary condition, based on the axial symmetry of the EPR spectra. These findings were supported by our DFT calculations on the model compound depicted in Fig. 9a and the parameters of the MM dihedral potentials collected in Table 3. The backscattering part of the EXAFS spectra also clearly favors a planar copper environment. The multiple scattering signal of EXAFS is maximized at an angle of 180° between the multiple scattering pathways where the atoms are placed in a linear fashion. In this context it is important to mention that the position of the His imidazole ring can be determined by ENDOR and EXAFS independently. EXAFS requires the imidazole ring at a position where a Cu–N_δ distance of 1.93 Å can be maintained, and, owing to the large multiple scattering fraction, the imidazole ring has to be situated in the same plane as the four Cu ligands.

The ESEEM measurements also show a His ligand and, when the imidazole ring is placed in the same way as demanded by EXAFS, a proton is positioned at 3.1 Å distance in the ligand plane (compare Fig. 8). This result is fully compatible with the ENDOR spectrum at $B = 328.3$ mT (resonances at 11 and 17 MHz) and clearly underlines the complementarity of ENDOR and EXAFS data. Our structural refinement excluded the N_ϵ of histidine as a ligand of Cu. The existence of an axial water molecule could be determined by our ENDOR experiments. Close proximity of the Trp side chain to the Cu in our structure is in agreement with fluorescence

Table 4 The application of the six different selections described in the text rule out a certain number of structure classes and a certain percentage of total structures that are given in the table. Results are presented for N_δ and N_ϵ ligation of the Cu^{2+}

	N_δ		N_ϵ	
	Number of classes	Total structures (%)	Number of classes	Total structures (%)
(1) Ligand distances	69	62.9	62	66.1
(2) Close atoms	60	69.9	74	71.6
(3) Planarity of ligation	29	36.8	43	52.9
(4) Histidine angle	21	58.0	–	–
(5) Force field violations	96	89.4	156	96.9
(6) Best 50% in total energy	0	50.0	0	50.0

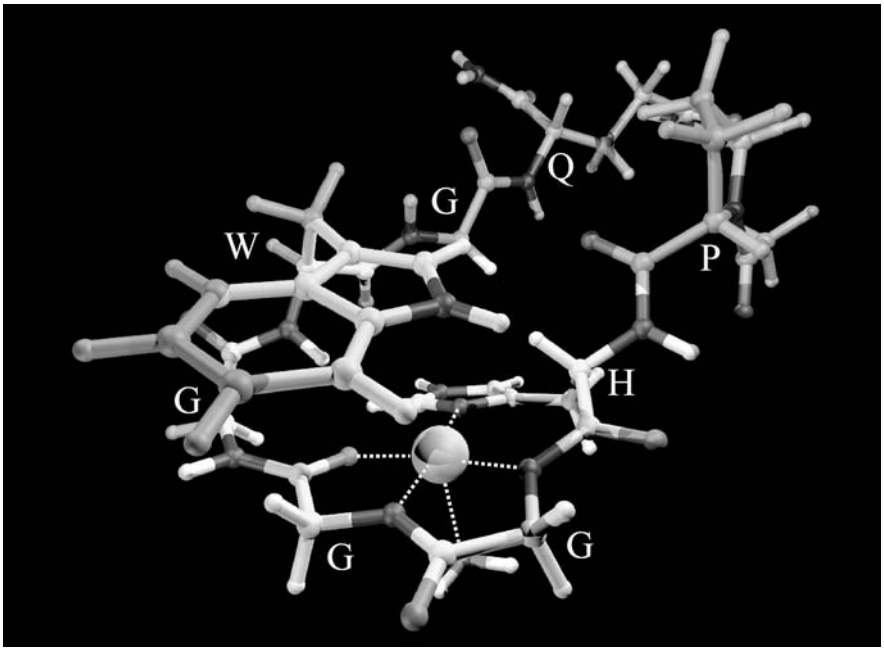

Fig. 10 Refined structure of the copper complexed prion protein octarepeat. The *bright part* of the figure includes all atoms which are in a sphere of 5 Å diameter around the copper. The spectroscopic methods which we used are sensitive to these positions. The rest of the complex is obtained via the MD simulations, taking into account standard geometries

(Hornshaw et al. 1995; Stöckel et al. 1998), Raman (Miura et al. 1999; Miura et al. 1996), NMR (Luczkowski et al. 2002) and CD (Hornshaw et al. 1995; Stöckel et al. 1998) data.

Concerning the copper complexation of the octarepeat sequence, various models have been proposed in the literature. Early models, like those from Stöckel et al. (1998) or Viles et al. (1999), cannot be compared with our model since they involve sequences of more than one octarepeat.

Quite consistent with our data is the structural model of Aronoff-Spencer et al. (2000), which was based mainly on CD and EPR spectroscopy performed in 25 mM NEM at pH 7.4. In this model the coordination sphere consists of three nitrogens and one oxygen, as indicated by EPR S- and X-band spectroscopy. Consequently, the Cu^{2+} ion was coordinated by a nitrogen of the imidazole ring and the backbone nitrogens of Gly3 and Gly4. So far, these data support our model. However, it was proposed that the Trp carbonyl oxygen acts as an oxygen ligand in the plane, based on experiments with short peptides where a similar copper ligation was found only for HGGGW and not for HGGG. This proposed ligation leads to a geometry in which the Trp side chain points relatively far away from the metal ion, a fact that does not agree with the fluorescence experiments (Hornshaw et al. 1995; Stöckel et al. 1998). It is also in contrast to NMR spectroscopy, which clearly revealed a close proximity of the Trp side chain to the copper ion (Luczkowski et al. 2002). According to our structure, a Trp side chain in close proximity of the copper ion is well compatible with the carbonyl oxygen of the Gly4 as the fourth metal ligand in the plane. In the course of our combinatorial approach, also the configuration of the Aronoff-Spencer model (Aronoff-Spencer et al. 2000) was analyzed. Compared to our final structure of Fig. 10, it showed high energy in the improper angles. In addition, we calculated EXAFS spectra of this structure. Owing to a poor agreement with our experimental spectra, the configuration was discarded.

In the NMR solution structure of the copper complex with the heptapeptide lacking the C-terminal Gln residue, the metal ion is coordinated by six instead of five atoms (Luczkowski et al. 2002). The three nitrogen ligands are identical to those of our structural model, but the imidazole is bound in an axial position and the complex has distorted tetragonal geometry. The model includes two more oxygen ligands close to the plane and one in an axial position derived from water molecules. In this model the Trp side chain is correctly positioned near the Cu center. The NMR spectra of the copper complex were recorded in the absence of buffer and the pH was adjusted to 7.4. This structural model does not agree with the EPR data that are best compatible with coordination by three nitrogens and one oxygen in a planar symmetric geometry. Moreover, the existence of two planar H_2O ligands can be excluded by our ENDOR measurements, since both deuterated and non-deuterated samples show the same resonances at the relevant field position. It is possible that solutions lacking NEM-like buffers result in different copper complexation. In our experience, the effect of buffer on the complex formation is substantial and similar findings have been reported previously (Viles et al. 1999).

A 3N-1O ligation has been found in the X-ray structure of the pentapeptide HGGGW-Cu^{2+} complex (Burns et al. 2002). The Cu center is coordinated in a roughly planar way. The N_δ of the imidazole ring acts as a nitrogen ligand as well as two amide nitrogens of the adjacent Gly residues 4 and 5. The carbonyl oxygen of

Gly4 is the fourth planar ligand. In the axial position, one water molecule coordinates the Cu and is stabilized by a hydrogen bond to the indole of the Trp6. Crystallization was done in 100 mM HEPES buffer at pH 7. A comparison of our structure of the octapeptide-Cu^{2+} complex with this X-ray structure reveals strong similarities in large parts, but also some discrepancies. The planar coordination of the Cu is identical and His2 shows the same conformation. However, our axial water molecule coordinates on the opposite site compared with the pentapeptide complex. The backbone atoms from His2 to Gly5 are very similarly arranged in both structures. Only the carbonyl oxygen of Gly5 points away from the center in our structure. As a consequence, the hydrogen bridge to a water molecule, as seen in the X-ray structure, becomes impossible. The conformation of the Trp6 differs completely in the two structures, a fact that can well be attributed to crystal packing effects. Indeed, the EXAFS spectra calculated for the pentapeptide complex were found to fit the experimental data much worse than the structure reported in Fig. 10.

EXAFS has also been used to determine the Cu binding geometry of the peptide KKRPKPWGQPHGGGWGQ, which contains one C-terminal octarepeat (Morante et al. 2003). However, the authors have used the X-ray structure of the pentapeptide-Cu(II) complex as a starting point for a merely local optimization of geometry, as opposed to our general approach where we make no a priori assumptions on the complex structure (except for the 3N-1O ligation). Although the structural model generated for the elongated peptide agrees in its overall geometry with our complex structure (Fig. 10), differences in the EXAFS spectra point to a significant influence of the additional amino acids.

Conclusions

Using EXAFS, EPR, ENDOR and ESEEM, together with computer calculations in an iterative way, it is possible to determine the structure of the environment of a metal ion within a sphere of 10 Å diameter with high precision. Applying this type of methodology, a highly reliable structure of the copper-bound octarepeat of the human prion protein was derived.

Acknowledgements This work was supported by the Bayerischer Forschungsverbund Prionen and the Bundesministerium für Bildung und Forschung.

References

Allen FH (2002) The Cambridge structural database: a quarter of a million crystal structures and rising. Acta Crystallogr Sect B 58:398–406

Arnesano F, Banci L, Bertini I, Felli IC, Luchinat C, Thompsett AR (2003a) A strategy for the NMR characterization of type II copper(II) proteins: the case of the copper trafficking protein CopC from *Pseudomonas syringae*. J Am Chem Soc 125:7200–7208

Arnesano F, Banci L, Bertini I, Mangani S, Thompsett AR (2003b) A redox switch in CopC: an intriguing copper trafficking protein that binds copper (I) and copper (II) at different sites. Proc Natl Acad Sci USA 100:3814–3819

Aronoff-Spencer E, Burns CS, Avdievich NI, Gerfen GJ, Peisach J, Antholine WE, Ball HL, Cohen FE, Prusiner SB, Millhauser GL (2000) Identification of the Cu^{2+} binding sites in the N-terminal domain of the prion protein by EPR and CD spectroscopy. Biochemistry 39:13760–13771

Binsted N, Strange RW, Hasnain SS (1992) Constrained and restrained refinement in EXAFS data analysis with curved-wave theory. Biochemistry 31:12117–12125

Bonomo RP, Impellizzeri G, Pappalardo G, Rizzarelli E, Tabbì G (2000) Copper(II) binding modes in the prions octapeptide PHGGGWGQ: a spectroscopic and voltammetric study. Chem Eur J 6:4195–4202

Brown DD (2001a) Prion and prejudice: normal protein and the synapse. Trends Neurosci 24:85–90

Brown DR (2001b) Copper and prion disease. Brain Res Bull 55:165–173

Brünger AT (1992) X-PLOR version 3.1. The Howard Hughes Medical Institute, Yale University, New Haven, Conn., USA

Brünger AT, Campbell RL, Clore GM, Gronenborn AM, Karplus M, Petsko GA, Teeter MM (1987) Solution of a protein crystal structure with a model obtained from NMR interproton distance restraints. Science 235:1049–1053

Burns CS, Aronoff-Spencer E, Dunham CM, Lario P, Avdievich NI, Antholine WE, Olmstead MM, Vrielink A, Gerfen GJ, Peisach J, Scott WF, Millhauser GL (2002) Molecular features of the copper binding sites in the octarepeat domain of the prion protein. Biochemistry 41:3991–4001

Cereghetti GM, Schweiger A, Glockshuber R, Van Doorslaer S (2001) Electron paramagnetic resonance evidence for binding of Cu^{2+} to the C-terminal domain of the murine prion protein. Biophys J 81:516–525

Comba P, Remenyi R (2002) A new molecular mechanics force field for the oxidized form of blue copper proteins. J Comput Chem 23:697–705

Fonda L (1992) Multiple scattering theory of X-ray absorption: a review. J Condens Matter 4:8269–8302

Frisch MJT, Schlegel GW, Scuseria HB, Robb GE, Cheeseman MA, Zakrzewski JR, Montgomery VG, Stratmann JA Jr, Burant RE, et al. (1998) Gaussian 98. Gaussian, Pittsburgh, Pa., USA

Garnett AP, Viles JH (2003) Copper binding to the octarepeats of the prion protein. Affinity, specificity, folding and co-operativity: insights from circular dichroism. J Biol Chem 278:6795–6802

Hasnain SS, Murphy LM, Strange RW, Grossmann JG, Clarke AR, Jackson GS, Collinge J (2001) XAFS study of the high-affinity copper-binding site of human $PrP^{91–231}$ and its low-resolution structure in solution. J Mol Biol 311:467–473

Hornshaw MP, McDermott JR, Candy JM, Lakey JH (1995) Copper binding to the N-terminal tandem repeat region of mammalian and avian prion protein: structural studies using synthetic peptides. Biochem Biophys Res Commun 214:993–999

Hurst GC, Henderson TA, Kreilick RW (1985) Angle-selected ENDOR spectroscopy. 1. Theoretical interpretation of ENDOR shifts from randomly orientated transition-metal complexes. J Am Chem Soc 107:7294–7299

Jackson GS, Murray I, Hosszu LLP, Gibbs N, Waltho JP, Clarke AR, Collinge J (2001) Location and properties of metal-binding sites on the human prion protein. Proc Natl Acad Sci USA 98:8531–8535

Kramer ML, Kratzin HD, Schmidt B, Römer A, Windl O, Liemann S, Hornemann S, Kretzschmar H (2001) Prion protein binds copper within the physiological concentration range. J Biol Chem 276:16711–16719

Lee PA, Beni G (1977) New method for the calculation of atomic phase shifts: application to extended X-ray absorption fine structure (EXAFS) in molecules and crystals. Phys Rev B 15:2862–2883

Lehmann S (2002) Metal ions and prion diseases. Curr Opin Chem Biol 6:187–192

Luczkowski M, Kozlowski H, Stawikowski M, Rolka K, Gagelli E, Valensin D, Valensin G (2002) Is the monomeric prion ocatopeptide repeat PHGGWGQ a specific ligand for Cu^{2+} ions? J Chem Soc Dalton Trans 2269–2274

MacKerell AD Jr, Bashford D, Bellott M, Dunbrack RL Jr, Evanseck J, Field MJ, Fischer S, Gao J, Guo H, Ha S, Joseph D, Kuchnir L, Kuczera K, Lau FTK, Mattos C, Michnick S, Ngo T, Nguyen DT, Prodhom B, Reiher I, Roux B, Schlenkrich M, Smith J, Stote R, Straub J, Watanabe M, Wiorkiewicz-Kuczera JY, Karplus DM (1998) All-atom empirical potential for molecular modeling and dynamics studies of proteins. J Phys Chem 102:3586–3616

Meneghini C, Morante S (1998) The active site structure of tetanus neurotoxin resolved by multiple scattering analysis in x-ray absorption spectroscopy. Biophys J 75:1953–1963

Miura T, Hori-i A, Takeuchi H (1996) Metal-dependent alpha-helix formation promoted by the glycine-rich octapeptide region of prion protein. FEBS Lett 396:248–252

Miura T, Hori-i A, Mototani H, Takeuchi H (1999) Raman spectroscopic study on the copper(II) binding mode of prion octapeptide and Its pH dependence. Biochemistry 38:11560–11569

Morante S, González-Iglesias R, Potrich C, Meneghini C, Meyer-Klaucke W, Menestrina G, Gasset M (2003) Inter- and intra-octarepeat Cu(II) site geometries in the prion protein: implications in Cu(II) binding cooperativity and Cu(II)-mediated assemblies. J Biol Chem 279:11753–11759

Nolting HF, Hermes C (1992) Documentation for the EMBL EXAFS data analysis and evaluation program package, EXPROG, release 1.0. EMBL, Hamburg, Germany

Pardi A, Billeter M, Wüthrich K (1984) Calibration of the angular dependence of the amide proton-C. J Mol Biol 180:741–751

Peisach J, Blumberg WE (1974) Structural implications derived from the analysis of electron paramagnetic resonance spectra of natural and artificial copper proteins. Arch Biochem Biophys 165:691–708

Pettifer RF, Hermes C (1985) Absolute energy calibration of X-ray radiation from synchrotron sources. J Appl Crystallogr 18:404–412

Rehr JJ, Albers RC (1990) Scattering-matrix formulation of curved-wave multiple-scattering theory: application to x-ray-absorption fine structure. Phys Rev B 41:8139–8149

Renner C, Fiori S, Fiorino F, Deluca D, Mentler M, Grantner K, Parak FG, Kretschmar HA, Moroder L (2004) Micellar environments induce structuring of the N-terminal tail of the prion protein. Biopolymers 73:421–433

Riek R, Hornemann S, Wider G, Glockshuber R, Wüthrich K (1997) NMR characterization of the full-length recombinant murine prion protein, *m*PrP(23–231). FEBS Lett 413:282–288

Sayers DE, Stern EA, Lytle FW (1971) New technique for investigating noncrystalline structures: Fourier analysis of the EXAFS. Phys Rev Lett 27:1204–1207

Steiner RA, Meyer-Klaucke W, Dijkstra BW (2002) Functional analysis of the copper-dependent quercetin 2,3-dioxygenase. 2. X-ray absorption studies of native enzyme and anaerobic complexes with the substrates quercetin and myricetin. Biochemistry 41:7963–7968

Stöckel J, Safar J, Wallace AC, Cohen FE, Prusiner SB (1998) Prion protein selectively binds copper(II) ions. Biochemistry 37:7185–7193

Van Doorslaer S, Cereghetti GM, Glockshuber R, Schweiger A (2001) Unraveling the Cu^{2+} binding sites in the C-terminal domain of the murine prion protein: a pulse EPR and ENDOR study. J Phys Chem B 105:1631–1639

Viles JH, Cohen FE, Prusiner SB, Goodin DB, Wright PE (1999) Copper binding to the prion protein: structural implications of four identical cooperative binding sites. Proc Natl Acad Sci USA 96:2042–2047

Whittal RM, Ball HL, Cohen FE, Burlingame AL, Prusiner SB, Baldwin MA (2000) Copper binding to octarepeat peptides of the prion protein monitored by mass spectrometry. Protein Sci 9:332–343

Wüthrich K (2003) NMR studies of structure and function of biological macromolecules. Biosci Rep 23:119–153